

Article

Removal of VOCs by Ozone: *n*-Alkane Oxidation under Mild Conditions

Alina I. Mytareva *, Igor S. Mashkovsky , Sergey A. Kanaev, Dmitriy A. Bokarev , Galina N. Baeva, Alexander V. Kazakov and Alexander Yu. Stakheev 

N.D. Zelinsky Institute of Organic Chemistry Russian Academy of Sciences, Leninsky Prospect 47, 119991 Moscow, Russia; im@ioc.ac.ru (I.S.M.); skanaev@ioc.ac.ru (S.A.K.); bokarev_d@mail.ru (D.A.B.); bg305@ioc.ac.ru (G.N.B.); ak@ioc.ac.ru (A.V.K.); st@ioc.ac.ru (A.Y.S.)

* Correspondence: aim@ioc.ac.ru

Abstract: Volatile organic compounds (VOCs) have a negative effect on both humans and the environment; therefore, it is crucial to minimize their emission. The conventional solution is the catalytic oxidation of VOCs by air; however, in some cases this method requires relatively high temperatures. Thus, the oxidation of short-chain alkanes, which demonstrate the lowest reactivity among VOCs, starts at 250–350 °C. This research deals with the ozone catalytic oxidation (OZCO) of alkanes at temperatures as low as 25–200 °C using an alumina-supported manganese oxide catalyst. Our data demonstrate that oxidation can be significantly accelerated in the presence of a small amount of O₃. In particular, it was found that *n*-C₄H₁₀ can be readily oxidized by an air/O₃ mixture over the Mn/Al₂O₃ catalyst at temperatures as low as 25 °C. According to the characterization data (SEM-EDX, XRD, H₂-TPR, and XPS) the superior catalytic performance of the Mn/Al₂O₃ catalyst in OZCO stems from a high concentration of Mn₂O₃ species and oxygen vacancies.

Keywords: ozone catalytic oxidation (OZCO); ozonation; volatile organic compounds (VOCs); *n*-alkane oxidation; manganese catalyst; air pollutants; air purification



Citation: Mytareva, A.I.; Mashkovsky, I.S.; Kanaev, S.A.; Bokarev, D.A.; Baeva, G.N.; Kazakov, A.V.; Stakheev, A.Y. Removal of VOCs by Ozone: *n*-Alkane Oxidation under Mild Conditions. *Catalysts* **2021**, *11*, 506. <https://doi.org/10.3390/catal11040506>

Academic Editors:
Jean-François Lamonier and
Annemie Bogaerts

Received: 31 March 2021
Accepted: 14 April 2021
Published: 16 April 2021

Publisher's Note: MDPI stays neutral with regard to jurisdictional claims in published maps and institutional affiliations.



Copyright: © 2021 by the authors. Licensee MDPI, Basel, Switzerland. This article is an open access article distributed under the terms and conditions of the Creative Commons Attribution (CC BY) license (<https://creativecommons.org/licenses/by/4.0/>).

1. Introduction

Volatile organic compounds (VOCs) are a large group of chemical compounds with boiling points below 260 °C; they include alkanes, alkenes, aromatic hydrocarbons, aldehydes, ketones, alcohols, etc. [1]. VOCs are considered major air pollutants because of their significant contribution to the formation of photochemical smog, tropospheric O₃ and secondary aerosols [2–5]. VOCs negatively affect human health because of their toxic, malodorous, mutagenic and carcinogenic nature [6]. The main anthropogenic sources of VOCs are vehicle exhaust fumes and emissions from chemical and power plants, petroleum refining, food and textile manufacturing, etc. [7]. Rapid urbanization and industrialization contribute to the growing emissions of VOCs into the environment. Therefore, the development of effective methods and materials for the abatement of VOCs is of significant importance.

Several technologies have been developed for VOC removal, including adsorption [8] and absorption [9] processes, thermal oxidation [1], photocatalytic decomposition [10–12], biological degradation [13], non-thermal plasma catalysis [14,15], catalytic combustion [7,16] and hybrid treatment [17,18]. However, insufficient selectivity and low energy efficiency limit their application. In recent years, ozone catalytic oxidation (OZCO) has attracted much attention due to its versatility in handling a range of organic emissions at relatively low operating temperatures [19–21].

Among various OZCO catalysts, supported MnO_x demonstrates excellent VOC oxidation performance [22–24]. Einaga et al. compared M/Al₂O₃ and M/SiO₂ (M = Mn, Fe, Co, Ni, Cu) according to their catalytic performances in OZCO [25,26]. It has been observed that Mn-containing catalysts are the most active for benzene and cyclohexane

oxidation. Huang et al. investigated ozone catalytic oxidation of benzene over Mn, Co, Cu, Ni, Zn and Ce supported on ZSM-5 [27]. It has been shown that MnO₂/ZSM-5 exhibits the best activity and CO₂ selectivity (100% and 84.7%, respectively) at room temperature. Gopi et al. studied the OZCO of toluene over Mn, Ce, Cu, Ag and Co metal oxides supported on 13X zeolite [28]. It was revealed that the activity of the catalysts decreases in the following order: Mn/13X > Ce/13X > Cu/13X > Ag/13X > Co/13X. Chen et al. studied the ozonation of chlorobenzene over manganese supported on different carriers (Al₂O₃, TiO₂, SiO₂, CeO₂, and ZrO₂) to reveal the effect of carrier on the catalytic performance of MnO_x in OZCO [29]. The authors found that Mn/Al₂O₃ exhibited the highest efficiency in chlorobenzene abatement.

The high efficiency of supported MnO_x catalysts in the OZCO of VOCs can be attributed to their ability in terms of O₃ decomposition [30]. It has been reported that highly reactive oxygen species such as atomic oxygen, peroxide, and OH radicals are formed (Equations (1)–(4)) on the surface of metal oxides as a result of O₃ decomposition [30–33]. These species can completely oxidize adsorbed VOCs to CO₂, even at room temperature (RT).



Recently, it was shown that OZCO may be considered a promising solution for the abatement of methane, which is difficult to destroy compared to alkenes and aromatics [34,35]. Thus, the conversion of methane achieved by catalytic oxidation using an air/O₃ mixture is almost four times higher than that using air only [35]. However, to the best of our knowledge, there are no available data on ozone catalytic oxidation of alkanes, which are the dominant VOCs generated by the petroleum industry [36,37]. Alkanes are also one of the major components among VOCs detected in vehicle exhaust [38]. Therefore, the aim of the present work was to investigate the possibility of ozone catalytic oxidation of *n*-butane (selected as a representative short-chain VOC molecule) at temperatures as low as 25–200 °C using an alumina-supported manganese oxide catalyst.

2. Results

2.1. Catalyst Characterization

Figure 1 shows the results of scanning electron microscopy (SEM) with energy-dispersive X-ray (EDX) spectroscopy analysis performed for the parent Al₂O₃ and the Mn/Al₂O₃ catalyst. The alumina (Figure 1a) has a relatively smooth surface. After loading 10 wt% Mn, the surface becomes rough with a number of defects (Figure 1b). The metal content is 9.4 wt% (Figure 1c), which is in a good agreement with data for inductively coupled plasma optical emission spectroscopy (ICP-OES) (see Section 4.1). The EDX mapping (Figure 1d) shows that Mn species are uniformly distributed on the catalyst surface.

X-ray powder diffraction (XRD) was used to identify the main MnO_x phases of the Mn/Al₂O₃ catalyst. Figure 2 shows XRD patterns of the parent alumina and the catalyst. The characteristic reflections of γ-Al₂O₃ (2θ = 37°, 46° and 67°) are detected in both spectra, which is in a good agreement with the published literature [23,29]. In the Mn/γ-Al₂O₃ pattern, typical reflexes of MnO₂ at 28.7°, 37.3°, 42.7° and 56.6° and Mn₂O₃ at 32.7° are observed, indicating that the two phases coexist [22,29]. The average particle sizes calculated from the diffraction peaks at 37.3° (MnO₂) and 32.7° (Mn₂O₃) using the Debye-Scherrer equation are 19.0 nm and 9.0 nm, respectively.

The redox properties of Mn/Al₂O₃ were investigated using temperature programmed reduction (H₂-TPR). A reduction profile composed of two peaks was observed (Figure 3a). The first peak, with a higher intensity at approximately 220–400 °C (T_{max} = 325 °C),

corresponds to the reduction of MnO_2 to Mn_2O_3 . The second peak, with $T_{\text{max}} = 431^\circ\text{C}$, is attributed to the reduction of Mn_2O_3 to MnO [39].

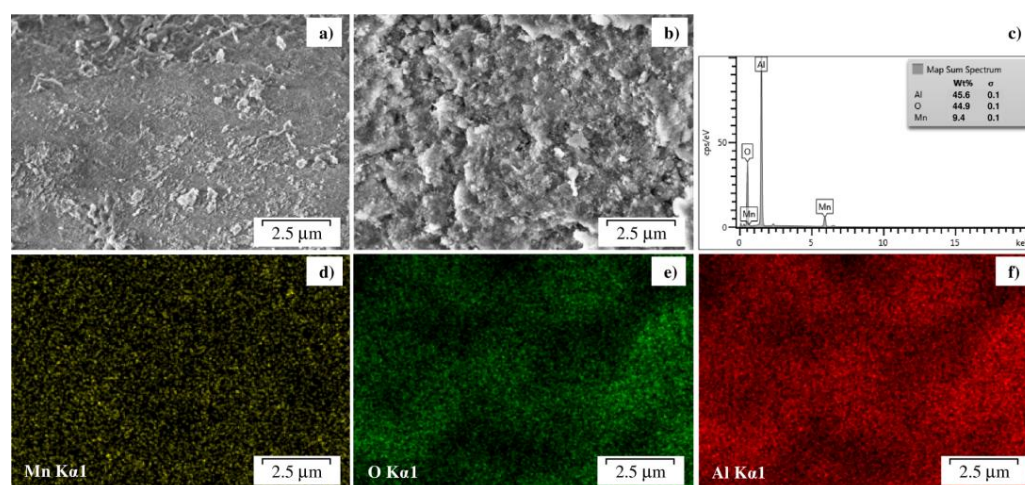


Figure 1. SEM micrographs of (a) the parent alumina and (b) the $\text{Mn}/\text{Al}_2\text{O}_3$ catalyst; (c) EDX spectrum and the elemental distribution maps of (d) Mn, (e) O and (f) Al for the $\text{Mn}/\text{Al}_2\text{O}_3$ catalyst.

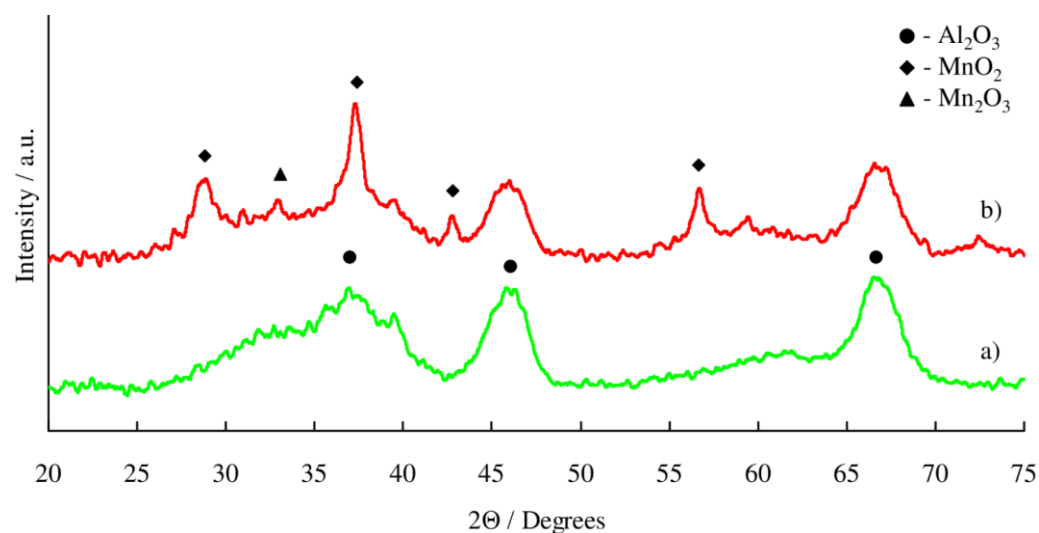


Figure 2. XRD patterns of (a) the parent alumina and (b) the $\text{Mn}/\text{Al}_2\text{O}_3$ catalyst.

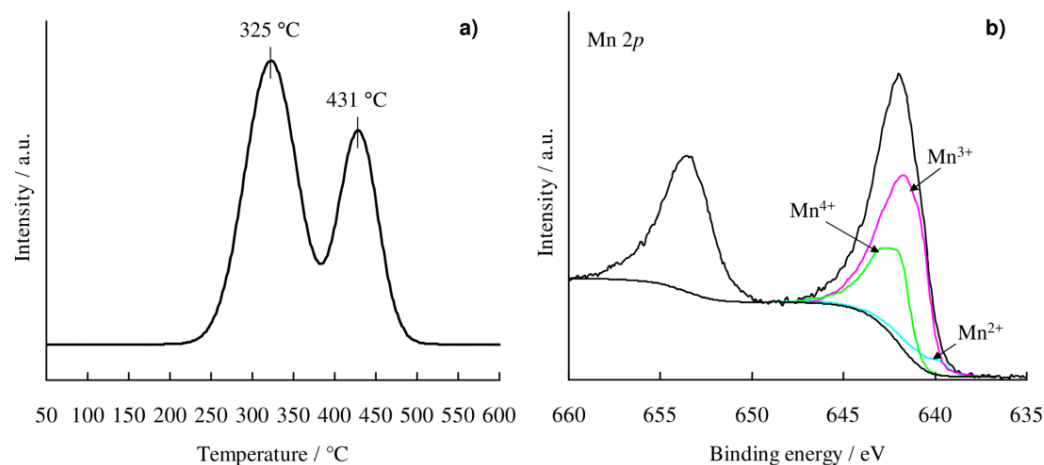


Figure 3. (a) H_2 -TPR and (b) Mn 2p XPS spectra of the $\text{Mn}/\text{Al}_2\text{O}_3$ catalyst.

To determine the valence states of the Mn atoms, the Mn/Al₂O₃ catalyst was examined by X-ray photoelectron spectroscopy (XPS). In the Mn 2p spectra (Figure 3b) of Mn/Al₂O₃, the peaks at 642.4, 641.8 and 640.8 eV were assigned to Mn⁴⁺, Mn³⁺ and traces of Mn²⁺, respectively [40–42]. The contents of Mn³⁺ and Mn⁴⁺ in the Mn/Al₂O₃ catalyst were approximately 69% and 31%, respectively.

2.2. Catalytic Activity

Three series of experiments were performed on the Mn/Al₂O₃ catalyst and the parent alumina: (a) *n*-C₄H₁₀ oxidation by air, (b) *n*-C₄H₁₀ oxidation by an air/O₃ mixture (OZCO), and (c) O₃ decomposition. In order to estimate the possible contribution of the gas-phase reactions, blank tests using an empty reactor were carried out.

2.2.1. *n*-C₄H₁₀ Oxidation

The blank oxidation reactions were carried out by air and air/O₃ mixture. The results obtained are summarized in Figure 4a. Evidently, the gas-phase oxidation of *n*-C₄H₁₀ by air does not proceed, even at temperatures as high as 350 °C. Contrarily, OZCO starts at 125 °C, and 80–90% conversion of *n*-C₄H₁₀ is achieved at 290–350 °C.

Over the Mn/Al₂O₃ catalyst, *n*-C₄H₁₀ can be oxidized by air; however, oxidation starts only at 225–250 °C, and at 350 °C the conversion does not exceed 20% (Figure 4a). In the course of OZCO, *n*-C₄H₁₀ is oxidized on the Mn/Al₂O₃ catalyst at 25 °C. Initially the conversion increases to 70% with the temperature and levels off at 85–200 °C (i.e., a plateau). At 200–250 °C, the conversion gradually decreases to ~55%; however, at 250–350 °C, it rises again to 85%.

It is known that the oxidation reaction may proceed not only on Mn-containing sites but also on the carrier surface. For this reason it was informative to evaluate the contribution of the parent Al₂O₃ (Figure 4a). The reaction between *n*-C₄H₁₀ and air does not proceed even at 350 °C. In the presence of O₃ the alkane is oxidized at 100 °C; however, the conversion is much lower than on Mn/Al₂O₃. This observation allows us to conclude that the activity of alumina surface in OZCO is negligible compared to MnO_x species.

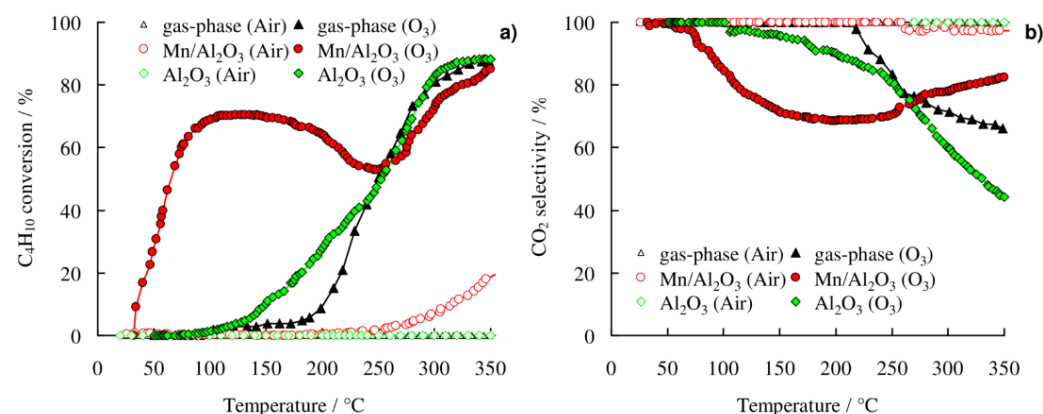


Figure 4. The gas-phase and catalytic oxidation of *n*-C₄H₁₀ by air and air/O₃ mixture: (a) *n*-C₄H₁₀ conversion and (b) CO₂ selectivity. Conditions: 100 ppm *n*-C₄H₁₀, air or 450 ppm O₃, balanced with N₂; F_{total} = 750 mL/min (GHSV = 155.000 h⁻¹).

Analysis of the reaction products reveals that *n*-C₄H₁₀ is completely oxidized by air over Mn/Al₂O₃; CO₂ selectivity is almost 100% (Figure 4b). When *n*-C₄H₁₀ reacts with both air and O₃ simultaneously, significant amounts of CO are formed. Thus, in the course of the gas-phase process and OZCO over the parent alumina, CO₂ selectivity gradually decreases with the increase in temperature, and at 350 °C it becomes 66% and 44%, respectively. In contrast, when *n*-C₄H₁₀ is oxidized by the air/O₃ mixture over the Mn/Al₂O₃ catalyst, CO mostly forms at relatively low temperatures (150–250 °C), and CO₂ selectivity is ca. 70%. At 350 °C the selectivity rises to ca. 85%. Other byproducts as well as a carbon deposition

on the catalyst surface were not detected, which is in good agreement with the high (>99%) carbon balance.

2.2.2. O₃ Decomposition

Since the enhancement of the oxidation efficiency in the presence of O₃ is attributable to a formation of highly reactive O atoms [29,32,33], catalytic O₃ decomposition (over Mn/Al₂O₃ or Al₂O₃) as well as gas-phase decomposition (in the empty reactor) was also studied in detail. The results obtained are shown in Figure 5. The gas-phase O₃ decomposition proceeds at relatively high temperatures (150–350 °C). In contrast, the reaction over the Mn/Al₂O₃ catalyst occurs at 25 °C, and the complete conversion of O₃ is achieved at 250 °C. On the parent alumina, O₃ decomposition starts only at temperatures above 100 °C.

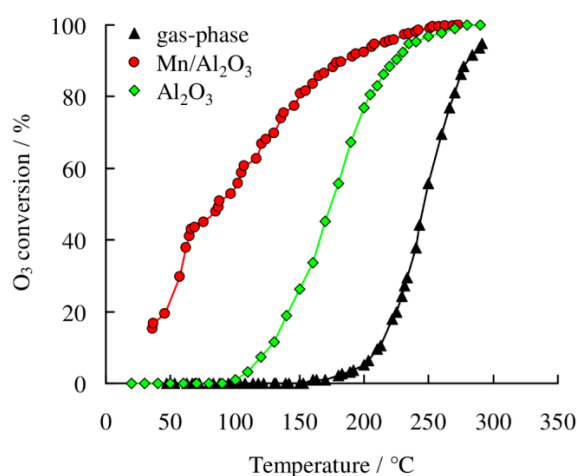


Figure 5. The gas-phase and catalytic O₃ decomposition. Conditions: 450 ppm O₃, balanced with N₂; F_{total} = 750 mL/min (GHSV = 155.000 h⁻¹).

2.2.3. The Effect of O₃/*n*-C₄H₁₀ Ratio on the Oxidation Efficiency

The effect of O₃ concentration on the *n*-C₄H₁₀ conversion on the Mn/Al₂O₃ catalyst was studied using feed gas containing different concentrations of O₃ (0–800 ppm) while keeping the *n*-butane concentration constant (100 ppm). Thus, the O₃/*n*-C₄H₁₀ ratio varies from 0 to 8. The results are summarized in Figure 6. The increase of *n*-butane conversion with O₃ concentration is observed. The complete conversion is obtained at 125 °C using an O₃/*n*-C₄H₁₀ ratio of eight.

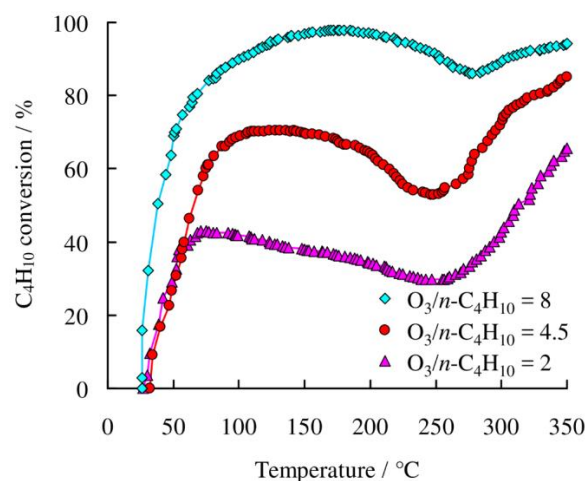


Figure 6. The OZCO of *n*-C₄H₁₀ at different O₃/*n*-C₄H₁₀ ratios. Conditions: 100 ppm *n*-C₄H₁₀, 200–800 ppm O₃, balanced with N₂; F_{total} = 750 mL/min (GHSV = 155.000 h⁻¹).

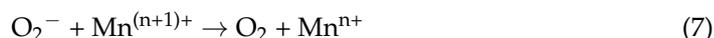
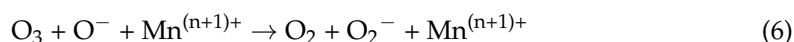
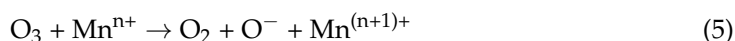
3. Discussion

3.1. Structure of Mn/Al₂O₃ Catalyst

The characterization data suggest that the Mn/Al₂O₃ catalyst contains a mixture of manganese oxides. The XRD pattern (Figure 2) shows pronounced peaks of MnO₂ along with a weak peak of Mn₂O₃, indicating that both oxide phases coexist in the catalyst [22,29]. The broadness of the MnO₂ peaks allows us to suggest that the oxide particles have poor crystalline structure and may contain structural defects, including oxygen vacancies. Low intensity of the Mn₂O₃ peak indicates that the oxide phase is well dispersed on alumina surface.

The H₂-TPR study of Mn/Al₂O₃ reveals an O/Mn stoichiometry of 1.71. This result agrees well with the XRD data, indicating the coexistence of MnO₂ and Mn₂O₃ in the catalyst. Based on the assumption that all MnO_x species are totally reduced to MnO, we estimate that the catalyst contains ca. 58% of Mn³⁺ and ca. 42% of Mn⁴⁺ species. Similar results were obtained by XPS, which shows that the surface of the Mn/Al₂O₃ catalyst is enriched with Mn³⁺ species.

The data obtained are in good agreement with previously reported results. Thus, it was shown repeatedly that the oxidation state of Mn species in Mn/Al₂O₃ catalysts with a low Mn loading (<10 wt%) is close to Mn³⁺, while at higher Mn loading (≥10 wt%) it tends to Mn⁴⁺ [22,26]. As reported in the literature [23,43], manganese in a low oxidation state is preferable for OZCO since it can transfer electrons to O₃ more readily (Equations (5)–(7)), thus facilitating O₃ decomposition.



It is known that the structural defects of MnO₂, such as oxygen vacancies, also favor OZCO due to their activity in O₃ decomposition. According to the mechanism proposed in the literature [30,44–47], O₃ molecules are adsorbed on the oxygen vacancies to form highly reactive oxygen species (O²⁻, O₂²⁻, O⁻), which readily react with VOC molecules. Thus, it has been reported that the high catalytic activity of the Mn-Ag/HZSM-5 for toluene oxidation by ozone is attributed mainly to the abundant oxygen vacancies presented on the catalyst surface [48].

3.2. Catalytic Activity

It was shown that oxidation of *n*-C₄H₁₀ is significantly accelerated in the presence of small amounts of O₃ (Figure 4a). The pronounced positive effect of O₃ addition is observed in the both gas-phase and catalytic reactions. Thus, the oxidation of *n*-C₄H₁₀ by air in the gas-phase and on the parent alumina does not proceed, even at temperatures as high as 350 °C. On the Mn/Al₂O₃ catalyst, only a minor conversion is observed. O₃ promotes oxidation in the gas-phase and on the alumina; the OZCO starts at 100–125 °C, and near-complete conversion is achieved at 300–350 °C. The effect of O₃ is significantly more pronounced when the reaction proceeds on the Mn/Al₂O₃ catalyst. In this case, the light-off temperature of the *n*-C₄H₁₀ oxidation decreases from 250 °C to 25 °C.

It was found that the behavior of *n*-butane oxidation is correlated with the O₃ decomposition process. Thus, it was observed that O₃ readily decomposes over the Mn/Al₂O₃ catalyst at 25 °C, the same temperature the *n*-C₄H₁₀ oxidation by air/O₃ mixture begins (Figures 4a and 5, respectively). Similar parallels of light-off temperatures have been observed when O₃ decomposition and *n*-C₄H₁₀ oxidation proceed in the gas-phase (at 150 °C) or over the alumina surface (at 100 °C). The results obtained are consistent with the published data [49]. Thus, it was found that at low temperatures the activation energy of benzene oxidation by O₃ is similar to that of O₃ decomposition, which suggests that O₃ decomposition can be considered as the rate-determining step of the oxidation process.

Comparative analysis of the conversion profiles obtained during the $n\text{-C}_4\text{H}_{10}$ OZCO and O_3 decomposition (Figures 4a and 5) allows us to suggest that the alkane is oxidized over $\text{Mn}/\text{Al}_2\text{O}_3$ in two stages. In the first stage (25–250 °C) the reaction proceeds mainly over MnO_x species, because the contribution of the alumina and the gas-phase reaction is negligible. The $n\text{-C}_4\text{H}_{10}$ is readily oxidized by O_3 ; however, the maximum conversion does not exceed 70% at 85–200 °C. One of the possible reasons of the limitation is the consumption of active atomic oxygen species in the reaction with O_3 (Equation (2)), which results in O_2 formation [24,30,31]. Apparently, the contribution of this reaction becomes more pronounced at temperatures of 200–250 °C, and $n\text{-C}_4\text{H}_{10}$ conversion decreases to ~55%.

At 250–350 °C, $n\text{-C}_4\text{H}_{10}$ conversion rises again and reaches 85%. Comparison of the conversion profiles obtained in the gas-phase and over the $\text{Mn}/\text{Al}_2\text{O}_3$ catalyst allows us to suggest that at higher temperatures the gas-phase $n\text{-C}_4\text{H}_{10}$ oxidation by air/ O_3 mixture becomes the dominant catalytic pathway (Figure 4a). In addition, the $n\text{-C}_4\text{H}_{10}$ oxidation by air over $\text{Mn}/\text{Al}_2\text{O}_3$ may contribute at temperatures above 250 °C (Figure 4a). This fact is indicated by the higher CO_2 selectivity as compared to the selectivity in the course of the gas-phase process and OZCO over the parent alumina (Figure 4b).

It has been shown that higher O_3 concentration enhances the alkane oxidation efficiency (Figure 6). Thus, as the $\text{O}_3/n\text{-C}_4\text{H}_{10}$ ratio increases from two to eight, the maximum $n\text{-C}_4\text{H}_{10}$ conversion obtained at low temperature (25–220 °C) rises from 43% to 100%. At the same time the plateau becomes wider, the decrease of conversion becomes less significant. According to the literature [24,50], both results are due to the increased availability of the highly reactive oxygen species for the oxidation of $n\text{-C}_4\text{H}_{10}$ over MnO_x species.

4. Materials and Methods

4.1. Catalyst Preparation

The 10% $\text{Mn}/\text{Al}_2\text{O}_3$ catalyst was prepared by incipient wetness impregnation of commercial Al_2O_3 carrier (SASOL, Sandton, South Africa; $S_{\text{BET}} = 150 \text{ m}^2/\text{g}$, calcined at 550 °C for 4 h) by an appropriate amount of an aqueous solution of manganese (II) nitrate tetrahydrate ($\geq 97\%$, Sigma Aldrich, St. Louis, MO, USA). The catalyst was dried at room temperature overnight and calcined in air flow (550 °C, 3 h).

Mn content in the resultant $\text{Mn}/\text{Al}_2\text{O}_3$ catalyst was determined by inductively coupled plasma optical emission spectroscopy (ICP-OES) on a Perkin Elmer OPTIMA 2000 instrument (PerkinElmer Inc., Wellesley, MA, USA) and found to be 9.8 wt%.

4.2. Catalyst Characterization

The morphologies of the samples were studied using a Hitachi SU8000 field-emission scanning electron microscope (Hitachi, Tokyo, Japan). Before measurements the samples were mounted on a 25 mm aluminum specimen stub and fixed by conductive graphite adhesive tape. Images were acquired in secondary electron mode at a 2–20 kV accelerating voltage and at a working distance of 8–10 mm. The energy dispersive X-ray spectroscopy (EDX) of the samples was tested on the same SEM instrument equipped with an Oxford Instruments X-max EDX system (Oxford Instruments, Abingdon, OX, UK) to analyze the element distributions on the surface.

The crystallographic structure of the as-prepared catalysts was characterized by X-ray powder diffraction (XRD) using a D8 Advance diffractometer (Bruker AXS, Karlsruhe, Germany) with Bragg–Brentano geometry, Ni-filtered $\text{CuK}\alpha$ radiation, and LYNXEYE detector. The XRD patterns were recorded in the 2θ range 5–75° (scan rate 1.2°/min). Crystallographic parameters were calculated using the Rietan-FT software, which uses the Rietveld method.

H_2 -temperature programmed reduction (H_2 -TPR) was conducted on a USGA-101 instrument (Unisit, Moscow, Russia). The catalyst sample (100 mg) was pre-treated in Ar flow at 325 °C for 1 h and cooled down to RT. H_2 -TPR was carried out in a 5% H_2/Ar mixture at a flow rate of 30 mL/min. The temperature was ramped linearly from RT to 820 °C at a heating rate of 10 °C/min. The data were processed using the Data Treatment software of

the USGA-101 instrument. H₂ consumption was quantified using CuO (99.999%, Sigma Aldrich, St. Louis, MO, USA) and NiO (99.99%, Sigma Aldrich, St. Louis, MO, USA) standards. The H₂-TPR pattern of the Mn/Al₂O₃ catalyst was corrected using the H₂-TPR profile of the parent alumina as a background.

The X-ray photoelectron spectroscopy (XPS) spectra of the samples were recorded on Axis Ultra DLD spectrometer (Kratos Analytical Limited, Manchester, UK) with a monochromatic Al K α source (1486.6 eV, 150 W). The binding energies were calibrated with reference to the standard binding energy of contaminant carbon (C1s 284.5 eV).

4.3. Catalytic Tests

A scheme of the experimental setup is shown in Figure 7. *n*-butane was supplied from a 0.98% *n*-C₄H₁₀/N₂ cylinder (Linde Gas Rus, Balashikha, Russia) balanced with N₂. O₃ was generated from air using a Triozon OG-A0.5 ozone generator (TriOzon, Moscow, Russia). The concentrations of *n*-butane and O₃ were 100 and 450 ppm, respectively (unless otherwise stated). The total gas flow rate was 750 mL/min, with a corresponding gas hourly space velocity (GHSV) of 155.000 h⁻¹. The gas mixture passed through a reactor (a quartz tube with an inner diameter of 10 mm) with the catalyst inside (0.2 g, fraction 0.4–1.0 mm).

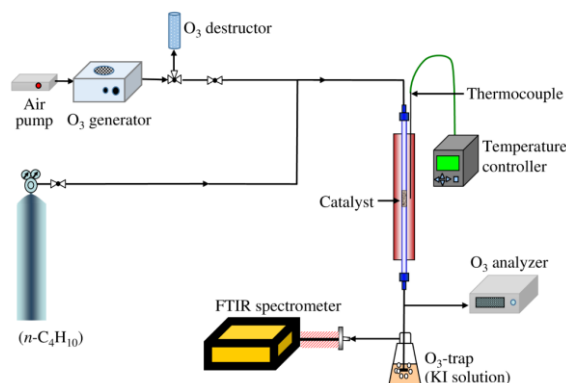


Figure 7. Scheme of the experimental setup.

The ozone concentration before and after the reactor was measured with an UV-100 ozone analyzer (Eco Sensors Division of KWJ Engineering Inc., Newark, CA, USA) in the range of 0–999 ppm with $\pm 2\%$ accuracy. For the correct analysis of the carbon-containing reaction products, an ozone trap with a saturated aqueous solution of KI was placed at the reactor outlet. An FTIR spectrometer Gasmet DX 4000 (Temet Instruments Oy, Helsinki, Finland) was used to detect concentrations of CO, CO₂, and *n*-C₄H₁₀.

Catalyst activity (conversion) was studied as a function of temperature ranging from 25 to 350 °C (temperature ramp of 5 °C/min). The conversions (*X*) of *n*-C₄H₁₀ and O₃ were calculated using the following equation:

$$X(\%) = \frac{C_{in} - C_{out}}{C_{in}} \times 100\%, \quad (8)$$

where C_{in} and C_{out} are the inlet and outlet concentrations of *n*-C₄H₁₀ and O₃, respectively.

Since only CO_x (CO, CO₂) were detected as the carbon-containing products of *n*-C₄H₁₀ oxidation, CO₂ formation was selected as a criterion for evaluating the effectiveness of the reaction. The CO₂ selectivity was calculated by the following equations:

$$CO_2 \text{ selectivity}(\%) = \frac{C(CO_2)_{out}}{(C(C_4H_{10})_{in} - C(C_4H_{10})_{out}) \times m} \times 100\%, \quad (9)$$

where C_{in} and C_{out} are the inlet and outlet concentrations of *n*-C₄H₁₀ and CO₂, respectively; *m* is the number of carbon atoms in the hydrocarbon (for *n*-C₄H₁₀, *m* = 4).

All carbon balances were in the range $(100 \pm 5)\%$.

5. Conclusions

The effect of O_3 on the efficiency of alkane oxidation was studied in details. It was shown for the first time that it is possible to oxidize short-chain VOCs by air/ O_3 mixture at ambient temperatures. It was observed that $n\text{-C}_4\text{H}_{10}$ reacted readily with O_3 over the $\text{Mn}/\text{Al}_2\text{O}_3$ catalyst at temperatures as low as $25\text{ }^\circ\text{C}$, and 80–100% conversion could be achieved in the temperature range $70\text{--}200\text{ }^\circ\text{C}$ ($O_3/n\text{-C}_4\text{H}_{10} = 8$).

Comparison of the catalytic and characterization data (SEM-EDX, XRD, H_2 -TPR, and XPS) revealed that superior catalytic performance of the $\text{Mn}/\text{Al}_2\text{O}_3$ catalyst in OZCO was due to high concentration of Mn_2O_3 species and oxygen vacancies.

The data obtained indicated that the oxidation pathway depends on the reaction temperature. Thus, at low temperatures $n\text{-C}_4\text{H}_{10}$ was oxidized by active oxygen, which was formed via O_3 decomposition over MnO_x species, while at $250\text{--}350\text{ }^\circ\text{C}$ the contributions of the gas-phase oxidation by air/ O_3 mixture and conventional oxidation by air over Mn-containing active centers became significant.

The findings of this study may contribute to the development of the efficient technologies for the low-temperature abatement of the short-chain hydrocarbons.

Author Contributions: Conceptualization, A.I.M. and A.Y.S.; investigation, D.A.B. and S.A.K.; data curation, I.S.M.; catalyst characterization, G.N.B. and A.V.K.; writing—original draft preparation, A.I.M.; writing—review and editing, A.Y.S. and D.A.B.; visualization, I.S.M.; supervision, A.Y.S. All authors have read and agreed to the published version of the manuscript.

Funding: Scientific Schools Development Program by Zelinsky Institute of Organic Chemistry is gratefully acknowledged.

Data Availability Statement: The data presented in this study are available on request from the corresponding author.

Acknowledgments: Authors gratefully acknowledge the Department of Structural Studies of N.D. Zelinsky Institute of Organic Chemistry for electron microscopy characterization.

Conflicts of Interest: The authors declare no conflict of interest.

References

1. Huang, H.; Xu, Y.; Feng, Q.; Leung, D.Y.C. Low temperature catalytic oxidation of volatile organic compounds: A review. *Catal. Sci. Technol.* **2015**, *5*, 2649–2669. [[CrossRef](#)]
2. Berezina, E.; Moiseenko, K.; Skorokhod, A.; Pankratova, N.V.; Belikov, I.; Belousov, V.; Elansky, N.F. Impact of VOCs and NO_x on ozone formation in Moscow. *Atmosphere* **2020**, *11*, 1262. [[CrossRef](#)]
3. Juráň, S.; Grace, J.; Urban, O. Temporal changes in ozone concentrations and their impact on vegetation. *Atmosphere* **2021**, *12*, 82. [[CrossRef](#)]
4. Juráň, S.; Edwards-Jonášová, M.; Cudlín, P.; Zapletal, M.; Šigut, L.; Grace, J.; Urban, O. Prediction of ozone effects on net ecosystem production of Norway spruce forest. *iForest-Biogeosci. For.* **2021**, *11*, 743–750. [[CrossRef](#)]
5. Wang, H.; Wang, Q.; Gao, Y.; Zhou, M.; Jing, S.; Qiao, L.; Yuan, B.; Huang, D.; Huang, C.; Lou, S.; et al. Estimation of secondary organic aerosol formation during a photochemical smog episode in Shanghai, China. *JGR Atmos.* **2020**, *125*, e2019JD032033. [[CrossRef](#)]
6. Okal, J.; Zawadzki, M. Catalytic combustion of butane on $\text{Ru}/\gamma\text{-Al}_2\text{O}_3$ catalysts. *Appl. Catal. B Environ.* **2009**, *89*, 22–32. [[CrossRef](#)]
7. Kamal, M.S.; Razzak, S.A.; Hossain, M.M. Catalytic oxidation of volatile organic compounds (VOCs)—A review. *Atmos. Environ.* **2016**, *140*, 117–134. [[CrossRef](#)]
8. Zhu, L.; Shen, D.; Luo, K.H. A critical review on VOCs adsorption by different porous materials: Species, mechanisms and modification methods. *J. Hazard. Mater.* **2020**, *389*, 122102. [[CrossRef](#)]
9. Ozturk, B.; Yilmez, D. Absorptive removal of volatile organic compounds from flue gas streams. *Process Saf. Environ. Prot.* **2006**, *84*, 391–398. [[CrossRef](#)]
10. Huang, Y.; Ho, S.S.H.; Lu, Y.; Niu, R.; Xu, L.; Cao, J.; Lee, S. Removal of indoor volatile organic compounds via photocatalytic oxidation: A short review and prospect. *Molecules* **2016**, *21*, 56. [[CrossRef](#)] [[PubMed](#)]
11. Higashimoto, S.; Katsuura, K.; Yamamoto, M.; Takahashi, M. Photocatalytic activity for decomposition of volatile organic compound on Pt-WO_3 enhanced by simple physical mixing with TiO_2 . *Catal. Commun.* **2019**, *133*, 105831. [[CrossRef](#)]

12. Sansotera, M.; Geran Malek Kheyli, S.; Baggioli, A.; Bianchi, C.L.; Pedferri, M.P.; Diamanti, M.V.; Navarrini, V. Absorption and photocatalytic degradation of VOCs by perfluorinated ionomeric coating with TiO₂ nanopowders for air purification. *Chem. Eng. J.* **2019**, *361*, 885–896. [[CrossRef](#)]
13. Zhang, S.; You, J.; Kennes, C.; Cheng, Z.; Ye, J.; Chen, D.; Chen, J.; Wang, L. Current advances of VOCs degradation by bioelectrochemical systems: A review. *Chem. Eng. J.* **2018**, *334*, 2625–2637. [[CrossRef](#)]
14. Cools, P.; De Geyter, N.; Morent, R. Plasma-catalytic removal of VOCs. In *Plasma Catalysis. Springer Series on Atomic, Optical, and Plasma Physics*; Tu, X., Whitehead, J., Nozaki, T., Eds.; Springer: Cham, Switzerland, 2019; Volume 106, pp. 145–180. [[CrossRef](#)]
15. Wang, B.; Xu, X.; Xu, W.; Wang, N.; Xiao, H.; Sun, Y.; Huang, H.; Yu, L.; Fu, M.; Wu, J.; et al. The Mechanism of non-thermal plasma catalysis on volatile organic compounds removal. *Catal. Surv. Asia* **2018**, *22*, 73–94. [[CrossRef](#)]
16. Yang, C.; Miao, G.; Pi, Y.; Xia, Q.; Wu, J.; Li, Z.; Xiao, J. Abatement of various types of VOCs by adsorption/catalytic oxidation: A review. *Chem. Eng. J.* **2019**, *370*, 1128–1153. [[CrossRef](#)]
17. Lee, J.E.; Ok, Y.S.; Tsang, D.C.W.; Song, J.; Jung, S.-C.; Park, Y.-K. Recent advances in volatile organic compounds abatement by catalysis and catalytic hybrid processes: A critical review. *Sci. Total Environ.* **2020**, *719*, 137405. [[CrossRef](#)]
18. Shu, Y.; Xu, Y.; Huang, H.; Ji, J.; Liang, S.; Wu, M.; Leung, D.Y.C. Catalytic oxidation of VOCs over Mn/TiO₂/activated carbon under 185 nm VUV irradiation. *Chemosphere* **2018**, *208*, 550–558. [[CrossRef](#)]
19. Aghbolaghy, M.; Ghavami, M.; Soltan, J.; Chen, N. Effect of active metal loading on catalyst structure and performance in room temperature oxidation of acetone by ozone. *J. Ind. Eng. Chem.* **2019**, *77*, 118–127. [[CrossRef](#)]
20. Fang, R.; Huang, H.; Huang, W.; Ji, J.; Feng, Q.; Shu, Y.; Zhan, Y.; Liu, G.; Xie, R. Influence of peracetic acid modification on the physicochemical properties of activated carbon and its performance in the ozone-catalytic oxidation of gaseous benzene. *Appl. Surf. Sci.* **2017**, *420*, 905–910. [[CrossRef](#)]
21. Sun, W.; Gao, X.; Wu, B.; Ombrello, T. The effect of ozone addition on combustion: Kinetics and dynamics. *Prog. Energy Combust. Sci.* **2019**, *73*, 1–25. [[CrossRef](#)]
22. Rezaei, E.; Soltan, J.; Chen, N. Catalytic oxidation of toluene by ozone over alumina supported manganese oxides: Effect of catalyst loading. *Appl. Catal. B Environ.* **2013**, *136–137*, 239–247. [[CrossRef](#)]
23. Zhu, B.; Li, X.-S.; Sun, P.; Liu, J.-L.; Ma, X.-Y.; Zhu, X.; Zhu, A.-M. A novel process of ozone catalytic oxidation for low concentration formaldehyde removal. *Chin. J. Catal.* **2017**, *38*, 1759–1769. [[CrossRef](#)]
24. Xi, Y.; Reed, C.; Lee, Y.-K.; Oyama, S.T. Acetone oxidation using ozone on manganese oxide catalysts. *J. Phys. Chem. B* **2005**, *109*, 17587–17596. [[CrossRef](#)] [[PubMed](#)]
25. Einaga, H.; Futamura, S. Comparative study on the catalytic activities of alumina-supported metal oxides for oxidation of benzene and cyclohexane with ozone. *React. Kinet. Catal. Lett.* **2004**, *81*, 121–128. [[CrossRef](#)]
26. Einaga, H.; Maeda, N.; Nagai, Y. Comparison of catalytic properties of supported metal oxides for benzene oxidation using ozone. *Catal. Sci. Technol.* **2015**, *5*, 3147–3158. [[CrossRef](#)]
27. Huang, H.; Ye, X.; Huang, W.; Chen, J.; Xu, Y.; Wu, M.; Shao, Q.; Peng, Z.; Ou, G.; Shi, J.; et al. Ozone-catalytic oxidation of gaseous benzene over MnO₂/ZSM-5 at ambient temperature: Catalytic deactivation and its suppression. *Chem. Eng. J.* **2015**, *264*, 24–31. [[CrossRef](#)]
28. Gopi, T.; Swetha, G.; Chandra Shekar, S.; Krishna, R.; Ramakrishna, C.; Saini, B.; Rao, P.V.L. Ozone catalytic oxidation of toluene over 13X zeolite supported metal oxides and the effect of moisture on the catalytic process. *Arab. J. Chem.* **2019**, *12*, 4502–4513. [[CrossRef](#)]
29. Chen, G.; Wang, Z.; Lin, F.; Zhang, Z.; Yu, H.; Yan, B. Comparative investigation on catalytic ozonation of VOCs in different types over supported MnO_x catalysts. *J. Hazard. Mater.* **2020**, *391*, 122218. [[CrossRef](#)]
30. Li, W.; Gibbs, G.V.; Oyama, S.T. Mechanism of ozone decomposition on a manganese oxide catalyst. 1. In situ Raman spectroscopy and Ab initio molecular orbital calculations. *J. Am. Chem. Soc.* **1998**, *120*, 9041–9046. [[CrossRef](#)]
31. Li, W.; Oyama, S.T. Mechanism of ozone decomposition on a manganese oxide catalyst. 2. Steady-state and transient kinetic studies. *J. Am. Chem. Soc.* **1998**, *120*, 9047–9052. [[CrossRef](#)]
32. Ramakrishna, C.; Shekar, S.C.; Gupta, A.K.; Saini, B.; Krishna, R.; Swetha, G.; Gopi, T. Degradation of diethyl sulfide vapors with manganese oxide catalysts supported on zeolite-13X: The influence of process parameters and mechanism in presence of ozone. *J. Environ. Chem. Eng.* **2017**, *5*, 1484–1493. [[CrossRef](#)]
33. Sekiguchi, K.; Kurita, Y.; Sankoda, K.; Namiki, N.; Yasui, F.; Tamura, H. Ozone catalytic oxidation of gaseous toluene over MnO₂-based ozone decomposition catalysts immobilized on a nonwoven fabric. *Aerosol Air Qual. Res.* **2017**, *17*, 2110–2118. [[CrossRef](#)]
34. Wan, M.P.; Hui, K.S.; Chao, C.Y.H.; Kwong, C.W. Catalytic combustion of methane with ozone using Pd-exchanged zeolite X: Experimental investigation and kinetics model. *Combust. Sci. Technol.* **2010**, *182*, 1429–1445. [[CrossRef](#)]
35. Hui, K.S.; Kwong, C.W.; Chao, C.Y.H. Methane emission abatement by Pd-ion-exchanged zeolite 13X with ozone. *Energy Environ. Sci.* **2010**, *3*, 1092–1098. [[CrossRef](#)]
36. Chen, C.-L.; Fang, H.Y.; Shu, C.-M. Source location and characterization of volatile organic compound emissions at a petrochemical plant in Kaohsiung, Taiwan. *J. Air Waste Manag. Assoc.* **2005**, *55*, 1487–1497. [[CrossRef](#)]
37. Ragothaman, A.; Anderson, W.A. Air quality impacts of petroleum refining and petrochemical industries. *Environments* **2017**, *4*, 66. [[CrossRef](#)]

38. Deng, C.; Jin, Y.; Zhang, M.; Liu, X.; Yu, Z. Emission characteristics of VOCs from on-road vehicles in an urban tunnel in Eastern China and predictions for 2017–2026. *Aerosol Air Qual. Res.* **2018**, *18*, 3025–3034. [[CrossRef](#)]
39. Ryu, H.W.; Song, M.Y.; Park, J.S.; Kim, J.M.; Jung, S.-C.; Song, J.-H.; Kim, B.-J.; Park, Y.-K. Removal of toluene using ozone at room temperature over mesoporous Mn/Al₂O₃ catalysts. *Environ. Res.* **2019**, *172*, 649–657. [[CrossRef](#)]
40. Langell, M.A.; Hutchings, C.W.; Carson, G.A.; Nassir, M.H. High resolution electron energy loss spectroscopy of MnO(100) and oxidized MnO(100). *J. Vac. Sci. Technol. A* **1996**, *14*, 1656–1661. [[CrossRef](#)]
41. Stranick, M.A. MnO₂ by XPS. *Surf. Sci. Spectra* **1999**, *6*, 31–38. [[CrossRef](#)]
42. Stranick, M.A. Mn₂O₃ by XPS. *Surf. Sci. Spectra* **1999**, *6*, 39–46. [[CrossRef](#)]
43. Radhakrishnan, R.; Oyama, S.T.; Chen, J.G.; Asakura, K. Electron transfer effects in ozone decomposition on supported manganese oxide. *J. Phys. Chem. B* **2001**, *105*, 4245–4253. [[CrossRef](#)]
44. Li, X.; Ma, J.; Yang, L.; He, G.; Zhang, C.; Zhang, R.; He, H. Oxygen vacancies induced by transition metal doping in γ -MnO₂ for highly efficient ozone decomposition. *Environ. Sci. Technol.* **2018**, *52*, 12685–12696. [[CrossRef](#)] [[PubMed](#)]
45. Zhu, G.; Zhu, J.; Jiang, W.; Zhang, Z.; Wang, J.; Zhu, Y.; Zhang, Q. Surface oxygen vacancy induced α -MnO₂ nanofiber for highly efficient ozone elimination. *Appl. Catal. B Environ.* **2017**, *209*, 729–737. [[CrossRef](#)]
46. Peng, B.; Bao, W.; Wei, L.; Zhang, R.; Wang, Z.; Wang, Z.; Wie, Y. Highly active OMS-2 for catalytic ozone decomposition under humid conditions. *Pet. Sci.* **2019**, *16*, 912–919. [[CrossRef](#)]
47. Ding, Y.H.; Zhang, X.L.; Chen, L.; Wang, X.R.; Zhang, N.; Liu, Y.F.; Fang, Y.Z. Oxygen vacancies enabled enhancement of catalytic property of Al reduced anatase TiO₂ in the decomposition of high concentration ozone. *J. Solid State Chem.* **2017**, *250*, 121–127. [[CrossRef](#)]
48. Li, J.; Na, H.; Zeng, X.; Zhu, T.; Liu, Z. In situ DRIFTS investigation for the oxidation of toluene by ozone over Mn/HZSM-5, Ag/HZSM-5 and Mn–Ag/HZSM-5. *Appl. Surf. Sci.* **2014**, *311*, 690–696. [[CrossRef](#)]
49. Naydenov, A.; Mehandjiev, D. Complete oxidation of benzene on manganese dioxide by ozone. *Appl. Catal. A Gen.* **1993**, *97*, 17–22. [[CrossRef](#)]
50. Kwong, C.W.; Chao, C.Y.H.; Hui, K.S.; Wan, M.P. Catalytic ozonation of toluene using zeolite and MCM-41 materials. *Environ. Sci. Technol.* **2008**, *42*, 8504–8509. [[CrossRef](#)]